# Molecular Rydberg states: Classical chaos and its correspondence in quantum mechanics

M. Lombardi, P. Labastie, M. C. Bordas, M. Broyer

# Molecular Rydberg states: Classical chaos and its correspondence in quantum mechanics

M. Lombardi
*Laboratoire de Spectrométrie Physique, Université Joseph Fourier-Grenoble 1, B. P. 87, 38402 Saint-Martin-d'Hères Cedex, France*

P. Labastie, M. C. Bordas, and M. Broyer
*Laboratoire de Spectrométrie Ionique et Moléculaire, Université Claude Bernard, 23, Bd du 11 Novembre 1918 69622 Villeurbanne, France*

(Received 25 January 1988; accepted 9 June 1988)

The Rydberg spectrum of $Na_2$ has been shown previously to alternate when increasing energy between "stroboscopic fringes" which correspond to a well known separable Hund's coupling case (a), and a complex, unidentifiable intermediate coupling. We use this system as a prototypic example to test some current ideas on the correspondence between classical chaos and properties of quantum spectra. We first determine the phase space structure and transition to chaos in classical mechanics. We then determine the change in line intensities and level spacing statistics in quantum mechanics. We show that this system has the expected behavior in the semiclassical limit in the presence of classical chaos, except for a peculiarity in level spacing statistics, but that this behavior is not a signature of chaos, since the same system shows similar behavior for some values of the parameters which correspond to a nonchaotic situation in classical mechanics. We discuss also some problems related to the nonvalidity of the semiclassical limit.

## I. INTRODUCTION

There has been a considerable amount of discussion in recent years about the correspondence in quantum mechanics of the well known chaotic behavior of classical low dimensionality systems.[1-3] In the present paper we want to critically discuss some ideas about this problem contained in the present literature, particularly those trying to infer from spectroscopic measures on a quantum system, the nature, chaotic or regular, of the classical system of the same Hamiltonian. To that purpose we display the results of a fully computable, classical and quantum mechanical system, which sheds new light on this problem because it is rather different from commonly studied systems.

Since most of the confusion about "quantum chaos" arises from ill defined questions, let us first define precisely what points we want to discuss. Let us start with an $n$ dimensional separable Hamiltonian, which can thus be written as a function of $n$ actions $I_n$ only:

$$\mathscr{H}_0 = \mathscr{H}_0(I_1,...,I_n).$$

Quantum mechanically to each action corresponds a good quantum number and levels are thus labeled by a set of $n$ good quantum numbers. Let us add now a Hamiltonian $\mathscr{H}_1$ which makes $\mathscr{H}_0 + \mathscr{H}_1$ nonseparable. $\mathscr{H}_1$ couples levels of $\mathscr{H}_0$. This has among others, two "obvious" consequences which have been the basis of two classes of techniques proposed to find a *signature* of chaos in quantum spectra:

(i) Level mixing: This produces a destruction of selection rules associated to $\mathscr{H}_0$ and increases the complexity of optical spectra (for example) used to probe the system by making "forbidden" lines to appear. This has led to a class of methods based on the statistics of line intensities.[4-6]

(ii) Level repulsion: This has led to another class based on a change of the statistics of level spacings.[7-9]

We will show in our example that while these two phenomena do appear in a semiclassical limit when the trajectories of the classical system of Hamiltonian $\mathscr{H}_0 + \mathscr{H}_1$ go from regular to chaotic, they are not a *signature* of classical chaos because a separable or nearly separable Hamiltonian with a negligible part of phase space invaded by chaotic trajectories do display similar phenomena in the quantum spectrum.

The example we will study is based on the experimental Rydberg spectrum of $Na_2$,[10] well understood quantum mechanically using multichannel quantum defect theory (MQDT).[11,12] In this experiment high Rydberg states of $Na_2$ are accessed by a two step laser excitation through a well defined rovibronic level of the $A\ ^1\Sigma$ electronic state. The virtue of this two step scheme for our study is that it enables the selection of a single $J$ in the intermediate state leading to only three possible $J$ in the Rydberg states (through $PQR$ branches), which have been sorted out through spectroscopic analysis. The final levels are thus a pure stretch of levels sharing the same good quantum numbers $J\pi$.

The basis of the MQDT analysis of this spectrum[10] is the following (Fig. 1): when the electron is far from the $Na_2^+$ ion core (of angular momentum $\mathbf{N}^+$) (i.e., "most of time" for a Rydberg electron), it senses only the spherically symmetric long range part of the ionic potential and its wave function is a Coulombic wave function of angular momentum $\mathbf{L}$ uncoupled to the rotational motion of the core. When the Rydberg electron is near the $Na_2^+$ core it senses, in addition, the cylindrically symmetric part of the $Na_2^+$ potential, which splits the $2L+1$ sublevels of the angular momentum $L$ into electronic levels labeled by the projection $\Lambda$ of $\mathbf{L}$ on the $Na_2^+$ axis: in the vector model of the molecule, $\mathbf{L}$ precesses rapidly around the $Na_2^+$ axis (Fig. 2). Near the bottom of the potential well, the electronic splitting between $\Lambda$ levels is much greater than the rotational splitting of the ion

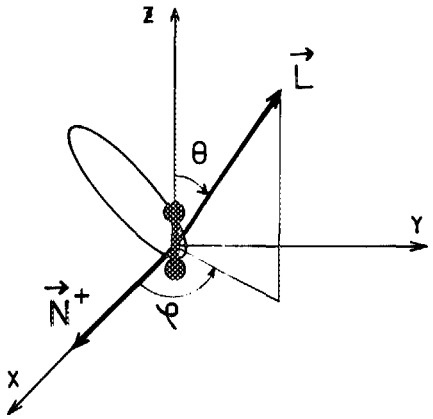


FIG. 1. Molecular reference frame. $N^+$ is the angular momentum of the $Na_2^+$ core. $(\theta,\varphi)$ are the polar angles of the angular momentum L of the electron with respect to $Oz$, $(\alpha,\beta)$ the polar angles of L with respect to $Ox$.

core. The wave functions are Hund's case (a) [or (b) if the total electron spin is zero] labeled by the principal quantum number $n$ of the Coulomb orbit, $\Lambda$, $J$, and also by $L$ in a simplified, experimentally justified, model we will use here, but $N^+$ is not a good quantum number. Their energy is

$$E^{(a)}_{nL\Lambda J} = -\frac{\mathrm{Ry}}{(n-\mu_\Lambda)^2} + B\,[J(J+1) + 1(1+1) - 2\Lambda^2],$$

where Ry is the Rydberg energy, $\mu_\Lambda$ the quantum defect of state $\Lambda$, and $B = 1/(2I)$ the rotational constant of the molecule. The intermediate state being a $A\Sigma^+$ state, only levels with $\Lambda = 0, \pm 1$ appear in the spectrum. When $n$ increases, the Rydberg splitting decreases until it is less than the rotational splitting or the core. Near the ionization limit, one might expect that the electron angular momentum L is completely uncoupled from the core's angular momentum $N^+$, so that the wave function is properly described by a Hund's case (d) wave function labeled by $n, L, N^+, J$ whose energy is given by

$$E^{(d)}_{nLN^+J} = -\frac{R}{(n-\mu)^2} + BN^+(N^+ + 1),$$

but $\Lambda$ is no longer a good quantum number.

This last fact destroys the effect of the $\Delta\Lambda = 0, \pm 1$ selection rule, so that every Rydberg level can be accessed from the $A\,^1\Sigma^+$, leading to an increase of complexity of the spectra.

The transition between the low and high energy regimes is thus expected to be a transition between two different Hund's coupling cases (a) and (d) due to a breakdown of the Born–Oppenheimer approximation for the Rydberg electron. In fact it has been shown[13] that the Hund's case (d) limit is never attained, the residual interaction being always too strong. Between these two easily predictables extremes, experiment has however found an unexpected phenomenon.[10] There appears periodically "clear zones" in the spectra. MQDT analysis of these spectra has shown that they correspond to periodic return to Hund's case (a) coupling which reestablish $\Delta\Lambda = 0, \pm 1$ selection rule and thus simplification of the spectrum. Such "resonance" occurs each time the period of an electronic orbit $T_e$ is an integer multiple of the period for a half-rotation of the $Na_2^+$ core $T_N/2$. The qualitative explanation given by the authors[10] is the following. At a resonance, the electron sees the core in the same position each time it returns, so the interactions with it are cumulative and the result is Hund's cases (a) coupling as at low energy when the core has not the time to rotate appreciably between two electron returns. To the contrary between resonances the electron receives at each interaction a rather random kick which destabilizes its orbit. The wave function in these intermediate states is nothing known: neither (a) nor (d) Hund's case coupling.

So the basic question which prompted us to do the present study is the following: does this phenomenon correspond to a transition to chaos with periodic reestablishment of regular trajectories corresponding to the existence of a separable or nearly separable dynamic approximation of the Hamiltonian at each resonance.

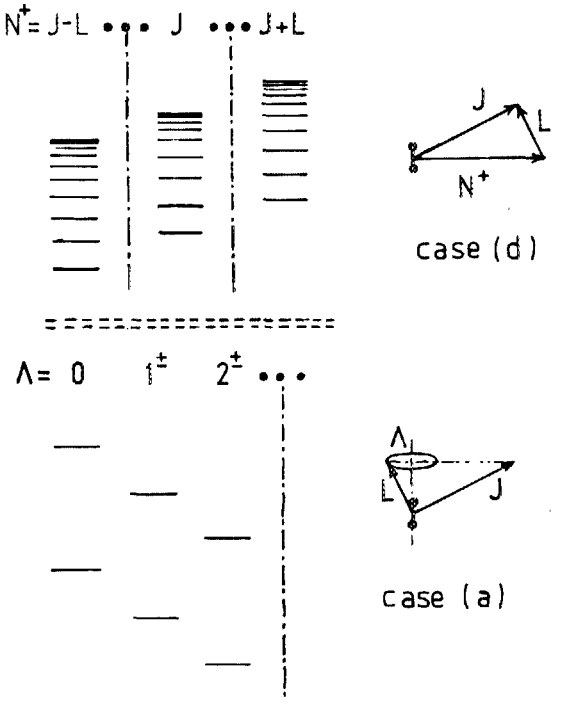


FIG. 2. Sketch of Rydberg series (left) and Hund's coupling cases (right).

## II. CLASSICAL TRAJECTORIES

### A. Principles

The classical trajectories are computed using the following model, which is the classical limit of the quantum MQDT approximation used to analyze the spectrum. When the electron is far from the core, it rotates freely on a Coulombic orbit of angular momentum L which is fixed in space. Meanwhile the $Na_2^+$ core rotates freely around its angular momentum $N^+$. Sticking to molecular frame (Fig. 1), L, seems thus to rotate around $N^+$ (which defines the molecular frame $x$ axis) in the opposite direction (clockwise). At each interaction with the core, L (supposed of constant magnitude) rotates around the $Na_2^+$ axis (which defines the molecular frame $z$ axis) by an angle $\delta\varphi = K\cos\theta = K\Lambda/L$

since $\Lambda$ is the projection of $\mathbf{L}$ into the $Na_2^+$ axis. We give in Appendix A a proof that this is the true semiclassical limit of the MQDT theory. $\delta\varphi$ must be an odd function of $\pi-\theta$ for symmetry reasons discussed in Appendix B. The $K\cos\theta$ value for $\delta\varphi$ is the simplest possibility, which corresponds to an experimentally plausible quantum defect

$$\mu_\Lambda = \mu_0 - \frac{K}{4\pi L}\Lambda^2.$$

The interaction conserves total angular momentum $\mathbf{J}=\mathbf{L}+\mathbf{N}^+$ and the total energy ($E = E_e + E_N$), sum of the electron and core energies, but neither $\mathbf{N}^+$ (it implies a kink to the molecular core) nor $E_N$ or $E_e$ separately. $\mathbf{N}^+$ may vary between $J-L$ and $J+L$, the rotational energy $E_N = |N^+|^2/2I$ and the period of the nuclei rotation $T_N = 2\pi I/N^+$ vary accordingly, and so do the electronic energy $E_e = E - E_N$ and the electronic period $T_e = 2\pi(-2E_e)^{-3/2}$. The motion in the molecular frame depends on two independent parameters $\theta$ and $\varphi$ (Fig. 1) which describe the relative position of $\mathbf{L}$ and $\mathbf{N}^+$, and one parameter which describes the position of the electron on the orbit. The fact that it does not depend on the position of the main axis of the orbit in the plane perpendicular to $\mathbf{L}$ is a (rather hidden) consequence of the approximation that makes $|\mathbf{L}|$ constant as discussed in Appendix A. The key property for the present discussion is that this classical model is the true limit for large quantum numbers of the MQDT approximation, not that it be a good approximation for a classical model of the molecule (which must fail somewhere since a molecule would not be stable in classical mechanics). We shall display Poincaré surface of section by plotting the polar angles $\theta$ and $\varphi$ of the $\mathbf{L}$ vector immediately after each collision with the core. This is a valid surface of section since $\varphi$ is canonically conjugate to $L_Z = \Lambda = L\cos\theta = -i\partial/\partial\varphi$. The equations for this $(\theta,\varphi)$ map resulting from a free orbit of the electron followed by a collision with the core are established in Appendix B. For better visualization the results are displayed on a (1,1,1) view of the unit sphere in Figs. 3–5.

### B. Results

All computations of this section correspond to $J = 20$, $L = 2$, $I = 10^6$ a.u., i.e., values of the right order of magnitude for the $Na_2$ experiments.

Figure 3 displays the transitions at low energy ($E = -0.1$ a.u.: corresponding to principal quantum number $n\sim 2$) between Hund's case (d) and Hund's case (a) when the coupling strength $K$ is increased. If $K = 0$ [Fig. 3(a)] $\mathbf{L}$ is fixed in absolute space and the molecular core rotates around its angular momentum. In molecular frame $\mathbf{L}$ rotates about $\mathbf{N}^+$ in opposite sense so that the trajectories are circles centered on the $Ox(\mathbf{N}^+)$ axis: These are pure Hund's case (d) trajectories. When increasing $K$ the trajectories near the positive $x$ pole (which is always a fixed point because it corresponds to a maximum value of $J = L + N^+$) expand along the $xz$ plane, split [Fig. 3(b)], and form two sets of closed loops which progressively migrate to the two $z$ poles [Fig. 3(c)]. For strong $K$[Fig. 3(d)] nearly all phase space is full of trajectories wounded around the $z$ axis: the $\delta\varphi$ motion induced by the collision with the core which produces a rotation around the $z$ axis has completely taken over the free rotation around the $x$ axis. This is pure Hund's case (a).

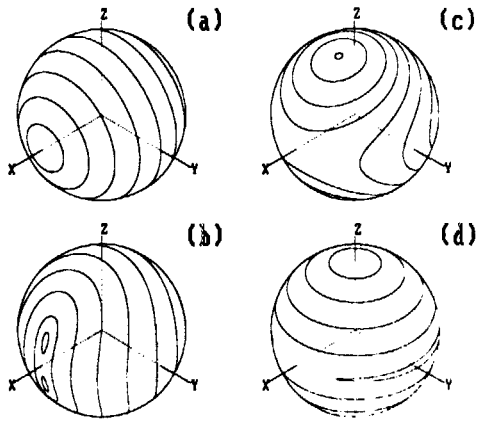


FIG. 3. Poincaré surface of section at low energy $E = -0.1$ a.u., for $L = 2$, $J = 20$, $I = 10^6$. The surface is a unit sphere in the molecular reference frame of Fig. 1 showing the positions of the electron's angular momentum immediately after a collision with the core. This figure displays the transition from case (d) to case (a) at low energy with increasing coupling (a) $K = 0$; (b) $K = -0.0012$; (c) $K = -0.005$; (d) $K = -1$.

Figure 4 displays the evolution with increasing energy for a medium coupling $K = -1$ [corresponding to Fig. 3(d)]. One has first an evolution which is nearly the same in

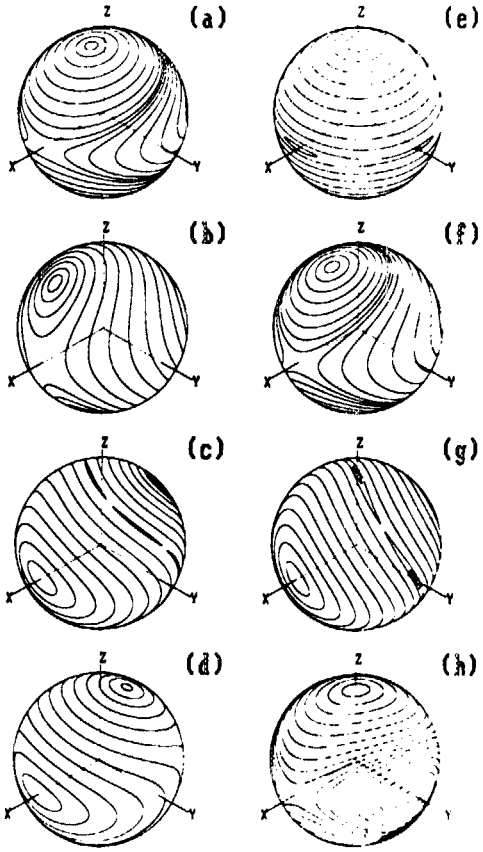


FIG. 4. Poincaré surface of section at medium coupling ($K = -1$) with increasing energy (labeled by the value of $T_e/T_N$ in the $yOz$ plane), for $L = 2$, $J = 20$, $I = 10^6$ (a) $T_e/T_N = 0.025$; (b) $T_e/T_N = 0.1$; (c) $T_e/T_N = 0.375$; (d) $T_e/T_N = 0.45$; (e) $T_e/T_N = 0.5$ (first resonance); (f) $T_e/T_N = 0.55$; (g) $T_e/T_N = 0.75$; (h) $T_e/T_N = 1$ (second resonance).

reverse order than in Fig. 3 [see Figs. 4(a)–4(c)], but the final result [Fig. 4(c)] despite the presence of orbits rotating around $Ox$, is much more complex than the simple Hund's case (d) of Fig. 3(a). Increasing once more the energy, one has another appearance of orbits which migrate to the pole $z$, but they start from the back side, negative $x$ axis [Fig. 4(d)]. At the first resonance [Fig. 4(e)], the Hund's case (a) of Fig. 3(d) is nearly recovered. Increasing further the energy [Figs. 4(f)–4(h)], the same kind of evolution is obtained until the second resonance. One sees however on Fig. 4(h) that there are in this case two classes of orbits: the first wound around the $Oz$ axis, corresponding the Hund's case (a) orbits, the second wound around the $Oy$ axis, corresponding to nothing known. The explanation of the difference between the first and the second resonance is the following: the value of $T_e/T_N$ which labels Figs. 3–5, and thus the resonance condition $T_e/T_N = k \times 0.5$ is valid usually only in the $yOz$ plane, where $\alpha = 0$ [see Fig. 1, Eq. (B2), and the sentence which follows it]. The resonance condition can however be valid for nearly the whole sphere if parameters $I$, $J$, and $L$ are chosen so that $\partial(T_e/T_N)/\partial(\cos\alpha) = 0$; i.e.,

$$(T_e/T_N) \times (J^2 - L^2) = (I/27)^{1/2}.$$

These parameters have been selected in Fig. 4 so that this condition is met for the first $T_e/T_N = 0.5$ resonance, giving the best resonance condition for Hund's case (a) return. In other cases, there remains always some orbits wound either around the $Oy$ axis, like in Fig. 4(h) or around the $Ox$ axis. Which of these two possibilities occurs depends both on the sign of the coupling parameter $K$ and on the value of $T_e/T_N$ with respect to the best resonance condition: Orbits are wound around $Oy$ if $K < 0$ and $T_e/T_N$ greater than the best, or if $K > 0$ and $T_e/T_N$ lower than the best, and around $Ox$ in the other cases.

Figure 5 displays the evolution at the first resonance ($T_e/T_N = 0.5$) with increasing coupling for the best resonance case. Starting from pure case (d) orbits [Fig. 5(a)] one has an increasing part of phase space invaded by case (a) orbits [Figs. 5(b)–5(d)] until it is nearly filled by such orbits. Increasing further the coupling there appears bifurcations giving complex structures near the equatorial plane. The chaos starts then from the equatorial plane for $K > 10$ and develops progressively toward the poles. For this best resonance case it is complete only for very high values of $K > 10^5$. For ordinary resonance cases like in Fig. 4(h), chaos develops first from the separatrix between the two kinds of orbits wound around $Oz$ and $Ox$ or $Oy$, for $|K| \approx 1$, and invades progressively the whole phase space which is filled for $|K|$ of the order of 100. If one makes the same study in between two resonances ($T_e/T_N = 0.75$), chaos begins at the same value of coupling ($K = -1$), but has invaded the whole phase space for $-K < 3.0$.

To display visually this phenomenon, one has plotted in Fig. 6 an indication of the degree of chaoticity as a function of the two parameters $T_e/T_N$ (which is a monotonic function of energy) and $K$. One sees clearly that each resonance ($T_e/T_N$ multiple of 0.5) gives a clear zone indicating resistance of the system to invasion by chaos. These clear zones correspond mainly to regular case (a) orbits wound around the $z$ axis. The parameters $I = 10^6$, $J = 10$, $L = 2$ have been chosen so that the best resonance case corresponds to $T_e/T_N = 2$. This is the explanation of the clear zone which extrapolates to $T_e/T_N = 2$ for $K = 0$.

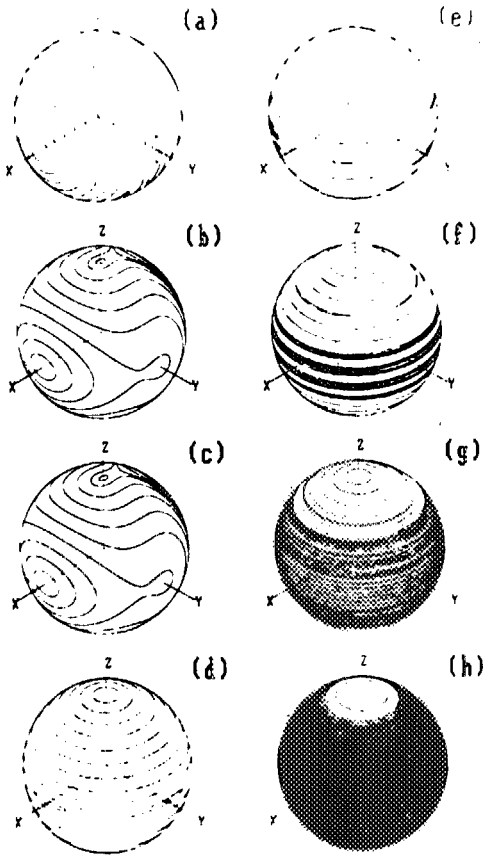


FIG. 5. Poincaré surface of section on the first resonance ($T_e/T_N = 0.5$) with increasing coupling for $L = 2$, $J = 20$, $I = 10^6$. (a) $K = -0.000\,001$; (b) $K = -0.0001$; (c) $K = -0.01$; (d) $K = -1$; (e) $K = -10$; (f) $K = -30$; (g) $K = -100$; (h) $K = -1000$.

### C. Conclusion

If the value of the coupling is strong enough (say $K = 3$), one sees in Fig. 6, the expected alternation between regular zones at low energy and at each resonance, and chaotic zones in between. However, Fig. 4 shows that for lower coupling, one has alternation between case (a) trajectories at low energy and at each resonance, and something which looks like case (d) trajectories but is definitively different in between. In this last situation, one will observe also in quantum mechanic spectra the periodic destruction and reestablishment of the simplicity of spectra due to case (a) selection rule. So the observed phenomenon, spectral complexity, may correspond to transition to chaos, but may also correspond to a drastic change of the structure of phase space. Spectral complexity due to loss of selection rules is a consequence of chaos but is not a *signature* of chaos.

## III. DISTRIBUTION OF LEVEL SPACINGS IN QUANTUM SPECTRUM

### A. Introduction: The technique of analysis

The second obvious consequence of breakdown of selection rules associated to the introduction of a nonseparable

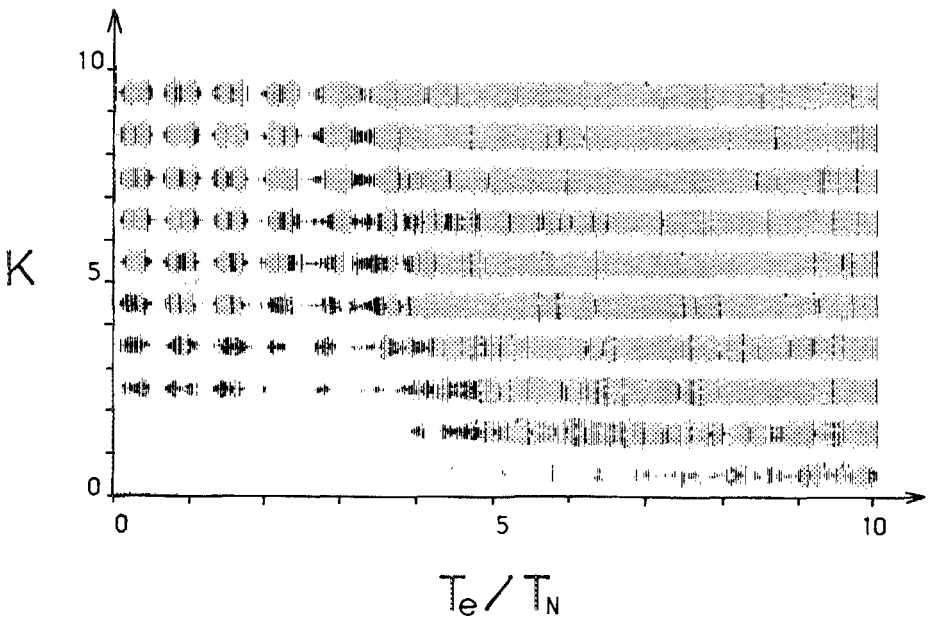


FIG. 6. Approximate degree of chaoticity as a function of $T_e/T_N$ (i.e., energy) and coupling $K$ for $L=2$, $J=10$, $I=10^6$. For a grid of values of $T_e/T_N$ and $K$, we have plotted bars whose vertical lengths are an approximate measure $F$ of chaoticity obtained as follows. One launches an orbit for a given value of $\theta$ and $\varphi$, computes the trajectory as a function of time, and Fourier transform the value of $\Lambda(t)$, giving $\Lambda(f)$ ($\Lambda=\cos\theta$ is the projection of $L$ on molecular axis). A regular orbit has a single frequency, a very chaotic orbit has a grassy frequency structure. A measure of the complexity of the spectrum is the ratio $F=|\int \Lambda(f)df|^2/\int \Lambda^2(f)df$. One should compute an average value of $F$ with respect to starting point. Here only one representative starting point $\theta=\pi/6$, $\varphi=\pi/2$ has been selected since we look only for a qualitative result and that trials with other (non singular) starting points give approximately the same results.

part $\lambda\mathscr{H}_1$ of the Hamiltonian is the phenomenon of level repulsion. When $\lambda$ increases, the first consequence is the lifting of degeneracies (described using degenerate perturbation theory). This effect is usually described by the change of the statistics of nearest neighbor spacings between an exponential Poisson distribution having a maximum at zero spacing (no repulsion) and a Wigner distribution which goes to zero for zero spacing.[14,15] If $\lambda$ increases further, repulsion occurs between levels more and more distant, which, being repelled from both sides, tend to be rather equally spaced. This phenomenon is frequently described by Mehta's $\Delta_3$ measure.[16] We will display here a much more significant measure of level spacings statistics, the Fourier transform of the energy spectrum

$$|C(t)|^2=\left|\int S\left(\frac{E}{h}\right)e^{-iEt/h}d\left(\frac{E}{h}\right)\right|^2.$$

It has indeed been shown[17] that this Fourier transform, when properly averaged is composed of two components (Fig. 7).

(a) A "fast component" which depends only on level density, not level spacings, and is thus useless for our purpose. In the case of the fast Fourier transform of a part of a theoretical "stick spectrum" of levels of same amplitude and constant density it reduces to the channel $O$, which contains the square $N^2$ of the total number of levels.

(2) A "slow component" which is the product of $N$ times the Fourier transform of a given level (which reduces to the constant 1 for a theoretical zero width stick spectrum) by the quantity

$$1-b_2(t)\times F,$$

where $b_2(t)$, the two level form factor, is the Fourier transform of the two level cluster function $Y_2(\Delta E/h)$[15,16] which describes the distribution of level spacings (the whole distribution, not just the nearest neighbor spacing). The quantity $F$ depends on fluctuation of line amplitude and is equal to one in the present theoretical stick spectra. Other measures

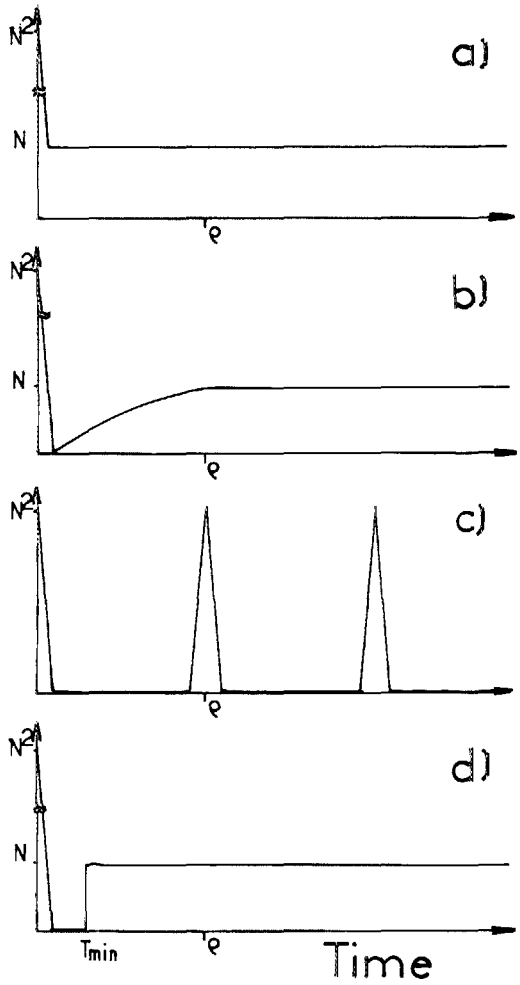


FIG. 7. Average Fourier transform of a quantum spectrum for four limit level statistics. (a) Purely random (Poisson) spectrum; (b) strongly coupled (GOE) spectrum; (c) picket fence (single harmonic oscillator); (d) generic case of a set of uncoupled anharmonic oscillator according to Berry, Ref. 9.

are exactly or approximately integrals over $1 - b_2(t)$. For example, the Mehta's $\Delta_3(r)$ measure can be written as

$$\Delta_3(r) = \int [1 - b_2(t)]K(r,t)dt$$

with a Kernel

$$K(r,t) = \frac{1}{(2\pi t)^2}[1 - F(y)^2 - 3F'(y)^2],$$

where

$$F(y) = \sin y/y \text{ and } y = \pi rt.$$

This formula is imbedded in a semiclassical derivation of Berry,[9] but it is perfectly general and can be derived directly by combining Eqs. (5.20) and (L4) of Ref. 15 and inverting the order of the integrations. The kernel $K(r,t)$ is plotted as a function of $t$ for some values of $r$ in Fig. 8. $\Delta_3(r)$ is thus a strong average of $1 - b_2(t)$, centered nearly at $1/r$, with a weight curve of area $r$ which extends at half-maximum from $1/2r$ to $2/r$ and has a long tail. This very strong smoothing increases the signal to noise ratio, but smoothes a lot of interesting details as will be shown later. The problem of nearest neighbor spacing is in principle more complicated because it depends not only on two level measures like $Y_2(\Delta E/h)$ or $b_2(t)$, but also on third and all higher order measure. In practice, in fact, it is determined mainly by the short range behavior of $Y_2$ or equivalently the asymptotic behavior of $1 - b_2(t)$. These two measures were popular in nuclear physics study[15] because the shortness of the stretch of levels available for a single nucleus ($< 100$) imposed very stringent limitation on the amount of statistical information which can be deduced from them, demanding use of extremely integrated, and thus very low information content techniques. The $\Delta_3$ statistics, e.g., was dubbed "the sharpest discrimination between Poisson and Wigner statistics," because it shows difference between them for the least possible number of levels. Such considerations are irrelevant in molecular studies where stretches of several thousands of levels are readily available: see, e.g., an application to acetylene SEP spectra in Ref. 18.

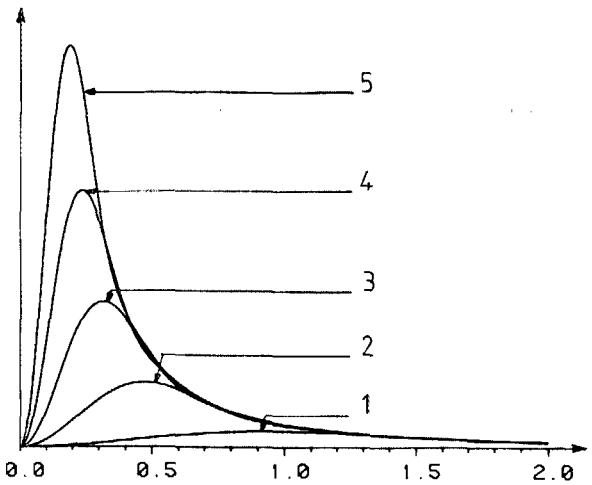


FIG. 8. Mehta's $\Delta_3(r)$ statistics are obtained by averaging the Fourier transforms of Fig. 7 with the weight factors described by the curves of this figure (labeled by the value of $r$).

### B. Prediction of random models and semiclassical rationale

Computation of the Fourier transform of a constant amplitude stick spectrum is the same as computation of the time evolution of a molecular wave function equal to $\Sigma_i |i\rangle$ at time $t = 0$ (where $|i\rangle$ are the eigenstates of $\mathscr{H}$). This discussion is thus very similar to the computations of radiationless theory of Bixon and Jortner[19] and Lahmani *et al.*[20] from which the names "fast" and "slow" components have been borrowed here. The only difference is that the zeroth order basis distinction between doorway states and hallway states made in these theories is irrelevant here. Results are sketched in Fig. 7. Figure 7(a) sketches the Fourier transform of a completely random set of levels, thought after the work of Berry and Tabor,[21] to represent the levels of a set of several uncoupled *anharmonic* oscillators. Notice however that the proof of randomness has been given only for the nearest neighbor spacing distribution. Figure 7(c) corresponds to a single harmonic oscillator, i.e., the Bixon and Jortner[19] model and displays characteristic recurrences. Figure 7(b) corresponds to the GOE,[15,16] i.e., a set of very strongly coupled levels, thought to correspond to a prototypic example of levels of a nonseparable Hamiltonian. For people used to radiationless theory, this last case is an intermediate case, the spacing being more regular than that of a pure random set but less regular than a strictly equidistant set, so that the various recurrences merge into a broad low amplitude plateau, leaving only a low emission hole between the initial fast decay and the first recurrence. The fact that the strong coupling case is not an extreme, but something intermediate between two prototypics separable cases is the basis of the explanation of various pitfalls in the following.

A very useful rationale to relate these properties of level spacings to Hamiltonian separability was given in semiclassical limit by Berry,[9] dwelling upon a theory of Gutzwiller[22] and Balian and Bloch.[23] These results properly translated into our language can be summarized by the following "cookbook recipe" to build the function $|C(t)|^2$. Launch orbits at every point $\mathbf{p}, \mathbf{q}$ in phase space compatible with the given value of energy and other good quantum numbers ($J$). Each time such an orbit closes, i.e., returns to the same point $\mathbf{q}$ with the same velocity $\mathbf{p}$, put a spike on $|C(t)|^2$. The single harmonic oscillator [Fig. 7(c)] gives thus regular spikes separated by the period $T$ of the oscillator. An uncoupled set of anharmonic oscillators gives the result of Fig. 7(d), somewhat different from Fig. 7(a). There is nothing in $|C(t)|^2$ (after the initial fast decay) before the orbit of shortest period $T_{\min}$ closes. Afterwards the closing of all random orbits gives an average constant as in Fig. 7(a). With a chaotic system, the number of closed orbits decrease drastically, giving the correlation hole observed in Fig. 7(b). More precisely the number of closed orbit increases linearly from zero with $t$ for low $t$. It is these conclusions we want to check and criticize by studying our $Na_2$ example.

### C. Results

We will compute the MQDT spectrum with the technique described in Ref. 10. However, for realistic values of the parameters, the number of levels contained in a reso-

nance is only a handful, which precludes a detailed statistical analysis of level spacings. To have accurate results, we have taken unrealistic (for $Na_2$) values of the parameters, which all increase the quantum numbers, going nearer to the semiclassical limit (and thus enabling a more meaningful comparison with Berry's semiclassical theory). We select $L = 10$, $J = 100$, even $J - L$ levels, $I = 2 \times 10^{11}$ (a.u.), so that the first resonance occurs for a principal quantum number $n = 1000$. It is thus possible to Fourier transform stretches of 500 levels at resonances and 1000 levels between resonances, for various values of the coupling parameter $K$. These values of parameters do not give a best resonance condition in classical mechanics but an ordinary resonance much like with the parameters of Fig. 6. Trial computations with a best resonance case ($J = 420$, all other the same) give no significant difference however.

Figure 9 displays some computed stick spectra. The abscissa is a rescaled energy corresponding to the principal quantum number of the series $N^+ = J-L$, which gives as we need a nearly constant level density (variation $< 1\%$ on a given stretch of levels). Figures 9(a) and 9(b) show that, in the spectrum near resonance for no coupling, levels occur in clumps of $L + 1 = 11$ levels corresponding to $L + 1$ series converging toward $N^+ = J - L$, $J - L + 2 ... J + L$ (see Fig. 2). Figure 9(c), no coupling also but off resonance, and Fig. 9(d), on resonance also but with strong coupling show no discernible structure.

Figure 10 displays Fourier transforms $|C(t)|^2$ on the first resonance for increasing coupling and Fig. 11 displays the same off resonance.

The result on resonance corresponds approximately to the Bixon and Jortner[19] model. There is not a single picket fence sequence, but $L + 1 = 11$ picket fence sequences of near equal spacing, which nearly coincide in the middle of the resonance. The spacings differ somewhat, however, because the sequences converge to different ionization limits (Fig. 2). This causes the recurrences to broaden and eventually to merge for times of the order $T \times T/\Delta T$, where $T$ is the average period, and $\Delta T$ the dispersion of the periods (i.e., the "anharmonicity" of the system). Since both Figs. 7(a) and 7(c) predict constancy of the average value of $|C(t)|^2$, we display in Fig 10(b) the result of Fig. 10(a) averaged (each point at time $t$ is the mean of points between $t - T/2$ and $t + T/2$). This shows definitively that there is an extra power on the first peaks, and that approximate constancy of the average is reached only for $t = 5$ (the level density being $t = 11$ in reduced units, due to the $L + 1 = 11$ sequences). The result off resonance, shows the same recurrence structure on $|C(t)|^2$, Fig. 11(a). There is no more an obvious clump structure in the spectrum, but a careful ex-

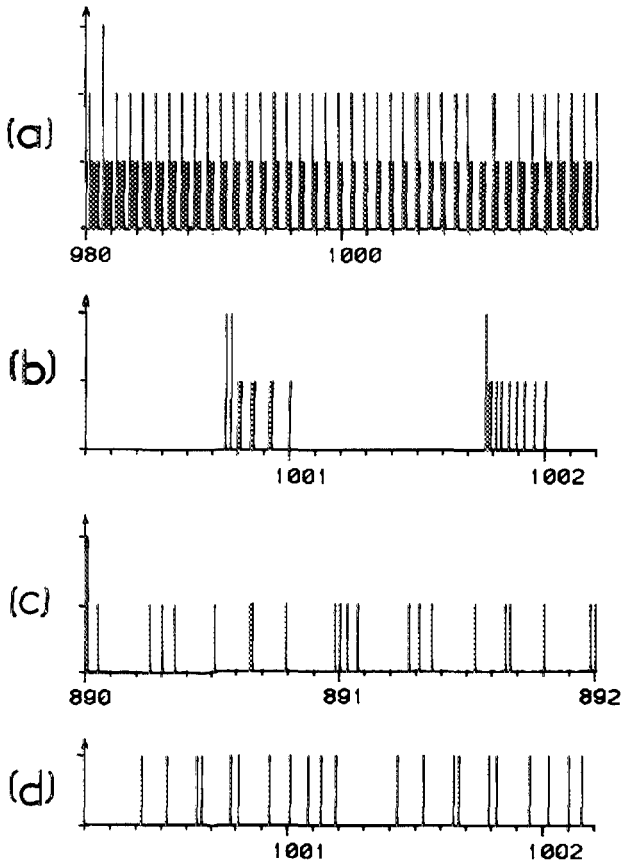


FIG. 9. Quantum spectra with MQDT approximation. $L = 10$ (even levels), $J = 100$, $2B = 1/I = 5 \times 10^{-12}$. The abscissa is $\nu_{90}$, the principal quantum number for the $J - L$ quantum series. (a) and (b) no coupling ($K = 0$) on first resonance ($T_e/T_N = 0.5$); (c) no coupling off resonance; (d) medium coupling $K = 1.25$, on resonance.

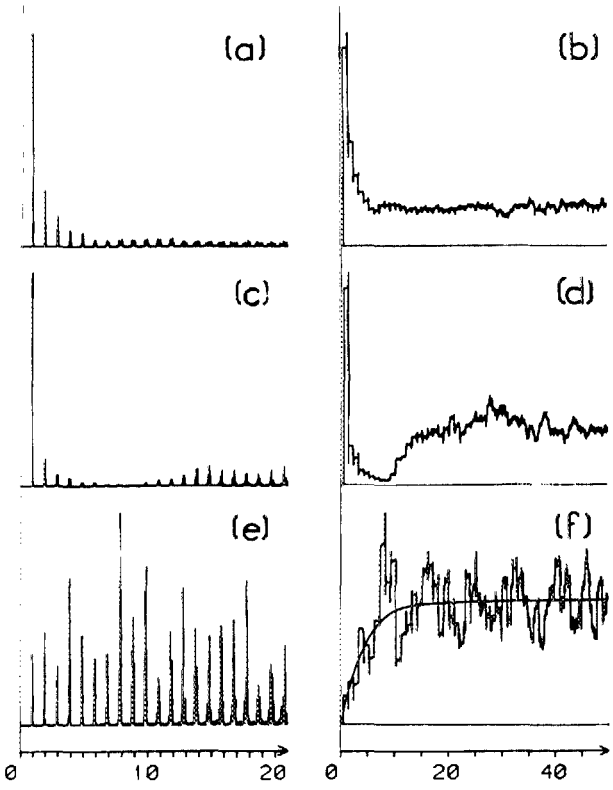


FIG. 10. Fourier transform of a quantum spectrum. On resonance ($T_e/T_N = 0.5$ in the middle of the spectrum). $\nu_{90} = 975$–$1025$. (a) No coupling ($K = 0$); (b) same integrated between $t - T_e/2$ and $t + T_e/2$, where $T_e$, the electron period is equal to the spacing between main peaks in (a); (c) $K = -0.25$; (d) $K = -0.25$ integrated like in (b); (e) $K = -15$; (f) $K = -15$ integrated like in (b).

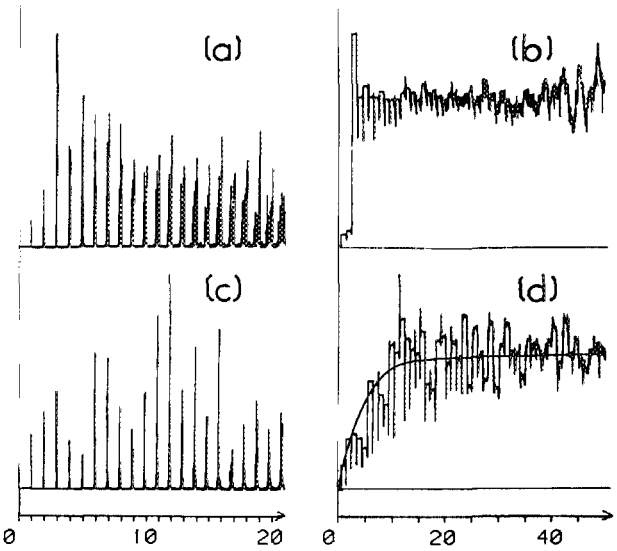


FIG. 11. Fourier transform of a quantum spectrum off resonance ($T_e/T_N = 0.35$ in the middle) $\rightarrow \nu_{90} = 840$–$940$. (a) $K = 0$; (b) $K = 0$ integrated as in Fig. 10(b); (c) $K = -15$; (d) $K = -15$ integrated.

amination of Figs. 3(c) and 3(d) shows that this small part of the spectrum is composed of two nearly identical patterns of 11 lines displaced by 1 in reduced units. This fact is the basis of the recurrence structures in Fourier transforms of Figs. 10 and 11. However, now Fig. 11(b) shows that the two first peaks are underweighted, and that constancy begins with the fourth peak. The meaning of these over and underweighting of first peaks is easily understood by thinking on Figs. 7(a)–7(b). The appearance of a hole at the origin in Fig. 7(b) with respect to Fig. 7(a) is due to the fact that the levels are more evenly spaced in a coupled system than in a random uncoupled one. Now Figs. 9(a)–9(b) show that levels on resonance are to the contrary more clumped than on random set, leading to a "correlation hump" instead of a "correlation hole." Now the disturbing observation is that the set of off resonance levels display a hole near the origin, indicating more regular than random long range spacings, much as what was expected in a strongly coupled system of Fig. 7(b).

Figures 10(e), 10(f), 11(c), and 11(d) now display results for strong coupling $K = 3$ which corresponds to a chaotic classical system at least off resonance. The two average curves tend as expected to the GOE results. What was not expected from Berry's theory is that the recurrence structure is conserved even in a completely chaotic classical situation. The reason of this failure is clear however. This system is unpredictable for infinite time, but it is fully predictable for times lengths $T_e$, when the electron is on its Rydberg orbit. The situation is in fact much similar to that found in billiards like the stadium which have been thoroughly investigated.[24] The movement is predictable between two strikes and unpredictable for long times. The difference in the present situation is that the time elapsed between two "strikes" is fairly constant. It varies in fact after each interaction because there is an exchange of energy between the electron and the core rotation, but since we have selected $J \gg L$, and that $N^+$ is constrained between $J - L$ and $J + L$, this variation is small in relative value. This near constancy of the period $T_e$ leads to the recurrences of the spectrum, the long term unpredictability leads to GOE envelope. Looking to $\Delta_3(r)$ measure on the same spectrum (Fig. 12), one finds the expected GOE behavior until a length of $r = 11$ average level spacings, corresponding to time $T_e$, and saturation for $r$ greater (the so-called "kink" phenomenon[25]). This saturation[9] is the consequence of the fact that the $\Delta_3$ weight function of Fig. 8 has a nearly constant long time tail part and that for values of $r$ greater than $1/T_e$, the increasing low times part of this function weighs nothing. Comparison of Fig. 12 with Figs. 11(c) and 11(d), which represent measures on the same system, illustrates how much information has been lost by using the extremely integrated $\Delta_3$ measure. The only remnant of the peaked structure are small glitches in Fig. 12 which are in fact numerical artefacts.

### D. Conclusion

The conclusion of this second part is much the same as that of the previous one. Chaos leads to transition to GOE envelope in $|C(t)|^2$, but purely separable systems [Fig. 3(d)] may lead to $|C(t)|^2$ which in the present case only looks like, but in other case may be identical to the GOE envelope. The level statistics are thus no more a *signature* of chaos.

## IV. DISCUSSION

Most of the systems used in previous studies, namely various two dimensional anharmonic coupled oscillators and various billiards, have the same global behavior. When increasing a parameter (frequently the energy, but sometimes rather a shape parameter), the phase space is progressively and monotonically invaded by chaos by destruction of invariant tori. But the general looking of the remaining tori and cantori is approximately conserved. Simultaneously one sees in quantum spectra loss of selection rules and onset of level repulsion. The present system is illuminating for two different reasons.

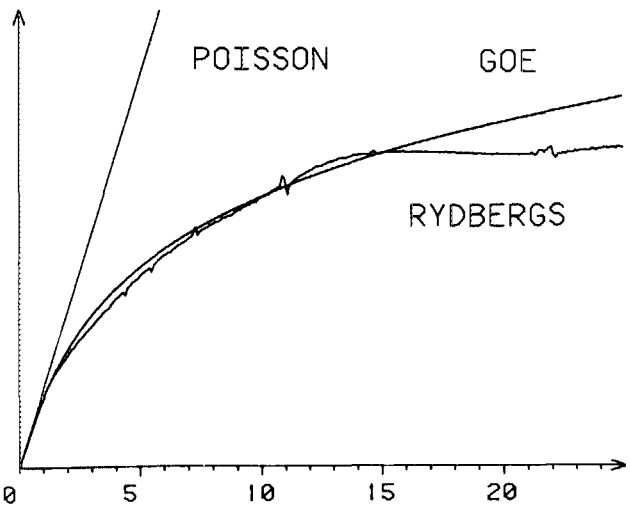


FIG. 12. $\Delta_3$ statistics for Poisson, GOE, and Rydberg's, $K = -15$, off resonance: $\nu_{90} = 840$–$940$ as in Fig. 11.

(i) For moderate values of the coupling parameter ($|K|<1$), it shows a periodic dramatic change of phase space structure when one increases the energy, with a fully negligible amount of phase space invaded by chaos. It shows definitely that loss of selection rules and its associated change in *statistics of line intensities* may have nothing to do with onset of chaos.

(ii) It is a very nearly, but not quite, harmonic system. This gives peculiarities in the *statistics of level spacings*, which are all related to the nongeneric behavior of harmonic systems discussed by Berry and Tabor.[21] We thus show, e.g., that the dual nature of this system, a regular clock at short times, but a fully chaotic system at long times (for $K$ big enough), leads to unexpected (but understandable) peculiarities in the spectrum, thought previously to be characteristic of regular systems, namely recurrences in time of $b_2(t)$, while keeping a GOE envelope of $b_2(t)$ which was expected for a chaotic semiclassical system. This result stresses the fact that classical chaos is an *infinite time* property of the systems, and that it gives no indication on how much time it needs to reach this asymptotic behavior.

All the preceding discussion pertains to what is expected in the semiclassical limit of quantum mechanics ($h\to 0$). This limit is quite valid in our case since we have used large quantum numbers: principal quantum number $n\approx 1000$, $L=10$, $J=100$. Another class of objections to the correspondence between classical chaos and level spacing statistics have been raised in the past. They correspond to the nonapplicability of the semiclassical limit in real quantum systems. This is thus not an objection to the Berry[9] theory, but it is of great importance in real situations. There are at least two clear cut reasons for divergences between semiclassical predictions and true quantum level spacing statistics, based on finite wavelength and finite time arguments.

(i) Finite wavelength. Why a finite quantum wavelength leads to a discrepancy between classical chaos and level spacing statistics can be understood very easily on a simple billiard example. Consider a circular (separable) billiard distorted by a very small granularity. This can be made analytically by suitably modifying the technique of Robnik,[26] using a conformal map from the unit circle by $Z=Az+B(zp+zq)$, with $p$ and $q$ very great integers, relative prime to avoid a discrete $C_k$ symmetry: an example is given on Fig. 13 for $p=q+1$. The mathematics will be given elsewhere but the results are self-evident. This billiard is chaotic for any energy as soon as it is nonconvex for at least one point.[27] This occurs for a very small amplitude $B/A$ of the granularity, of the order of $p^{-2}$, and cusps of the boundary occur for $B/A\approx p^{-1}$. This can be made arbitrarily small by increasing $p$ and/or $q$. Now quantum mechanics, having a finite wavelength which depends on energy, does not sense a granularity much smaller than the wavelength. The level spacing statistics is thus the statistics of a separable system up to an arbitrarily high energy, where the wavelength is of the order of the amplitude of the granularity, leading to onset of level repulsion, whereas the classical system is chaotic at any energy. It can even be very strongly chaotic if it approaches the cusp condition, where the time of divergence of trajectories is of the order of the time between two strikes on the boundary. This phenomenon is of course not an objection to the semi-classical theory of Berry[9] since it correspond to wavelength decreasing to zero.

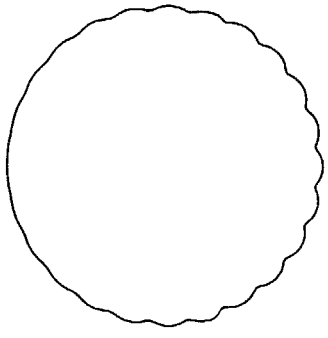

FIG. 13. Image of a circular billiard by the conformal map $Z=Az+B(zp+zq)$, with $p=25$, $q=26$, $B/A=0.01$.

Such a wavelength phenomenon is the gist of the dispute of Ref. 28 on the level statistics in HCN, where two different model Hamiltonians give the same quantum spectrum, consistent with experiment, and very different onsets of classical chaos. It has been eliminated in the present study by the way the model has been constructed. De Broglie wavelength enter in principle in the interaction between the outer electron and the core. Interaction occurs only for small partial waves, i.e., small $L$ values, leading to the possibility of separation of different $L$ multiplets and thus of approximate $L$ conservation in the actual quantum system, because of the small dimension of the core with respect to quantum wavelength. This would fail if $h$ would tend to zero consistently on all parts of the model. The MQDT approximation allows however to ignore such considerations in going to semiclassical limit using formula (A12) for the correspondence between quantum defects and classical behavior. This is ultimately the same kind of approximation as speaking of a circular billiard, ignoring that a true billiard has a granularity due at least to its atomic structure.

(ii) Finite Time. The fact that quantum mechanics can follow up classical mechanics only up to a finite time is popular in particular after the work of Casati and Guarneri[29] on the kicked rotator. Due to Heisenberg uncertainty relations, quantum mechanics must feel its quantum structure at least for a time of the order of $h$/average level spacing, and for very long times the fact that the Schrödinger equation is a linear equation which cannot lead to chaotic behavior must enter somewhere. This is the reason why the average curves of Figs. 7(a) and 7(b), which correspond to a separable and a nonseparable system, go to the same limit $N$ for times long with respect to $\rho$. This time limitation has another direct consequence on the present system. Consider what happens near the limit of a Rydberg series of given $N^+$ (Fig. 2). The number of levels of this series near this limit being infinite whereas all other series have only a finite number of levels in that neighborhood, one has for high enough principal quantum number a single isolated series. After unfolding the local level density one has a perfect picket fence spectrum, corresponding to the level statistics of a perfectly harmonic separable system, whereas the corresponding classical system is completely chaotic near the dissociation limit, as seen in Fig. 6. However, the time necessary for this classical system to become chaotic in this limit is the time between two interac-

tions with the core, which corresponds exactly to $h$/level spacing, so that the quantum system does not see it. Level statistics studies of Figs. 10 and 11 have been made for energies where the $L+1$ series are present and of nearly equal level density, so that the time necessary for the system to become chaotic is $1/(L+1)$ times $h$/average level spacing, enabling the level repulsion phenomenon to appear on the spectra.

Finally, notice that more complex combination of the same arguments enter in the explanation of theories of semiclassical quantization (for finite $h$) in chaotic domains by using a separable approximation to a nonseparable Hamiltonian,[30] in particular in the discussion of the effect of vague tori which constrain the classical trajectory on a nearly defined torus for a long but finite length of time. This has an application in the present system. It explains why in the situation of Figs. 4(f) and 4(g) where the layered structure of the chaotic part is an indication of the presence of a great number of cantori which confine for a long time the classical movement in the neighborhood of tori of given $L\cos\theta=\Lambda$ (with $L=10$ there are only 21 quantized values of $\Lambda$ on the sphere), the wave functions are Hund's case (a) wave functions, even if the statistics of level spacings [envelope of $b_2(t)$ in Fig. 10(f)] reflects the chaotic nature of the system.

## APPENDIX A: CLASSICAL LIMIT OF MQDT THEORY

MQDT theory separates space in two parts[10–13]:

(1) An outer part, where the Rydberg electron senses only the isotropic Coulombic part of the ion potential. In this part, the wave function is described by a Coulomb wave function quantized either in laboratory frame [Hund's case (d)] or in the molecular frame [Hund's case (a)]. This wave function is a combination of regular and irregular (at origin) solutions which vanish at infinity.

(2) An inner part, where the Rydberg electron senses the molecular core and where it is described in molecular frame.

The heart of MQDT analysis is to say that it is not necessary to plunge into the details of the core interaction. The effect of this interaction is given by a set of phase shifts on the surface separating the inner and outer parts. These phase shifts are identical to those defined in collision theory so that MQDT gives a unified way to treat collision states at positive energy and bound states (Rydberg states) at negative energy, if these phase shifts vary slowly with energy. This is actually the case, especially for high Rydberg states where the interaction of the accelerated electron with the core depends little on small velocity variations due to small energy changes which govern the long range behavior of the electron.

The outer part classical Coulomb orbit being well known, the only problem left to define the classical limit of MQDT is thus the classical limit of the phase shift description of the collision. The Schrödinger equation for the outer electron in a potential $U(z)$ of cylindrical symmetry around $Oz$ is (in atomic units)[31]

$$\left[\frac{d^2}{dr^2}+k^2-\frac{2}{r}-2U(r,\theta)-\frac{\mathbf{L}^2}{r^2}\right][r\psi(r,\theta,\varphi)]=0 \tag{A1}$$

with $E=k^2/2$.

The asymptotic form of the wave function is[31]

$$\psi(r,\theta,\varphi)=\sum_{L,m}Y_L^m(\theta,\varphi)a_{Lm}\frac{u_L^{(-)}(r)-e^{2i\delta_{Lm}}e^{2i\sigma_L}u_L^{(+)}(r)}{kr}, \tag{A2}$$

where $u_L^{\pm}(r)$ are ingoing and outgoing Coulomb wave functions, $\sigma_L=\arg\Gamma(1+L+i/k)$ is the Coulomb phase shift which leads to the Rutherford deviation, the potential phase shift $\delta_{Lm}$ goes to zero and $a_{Lm}$ becomes independent of $m$ if $U(r,\theta)\to 0$. The fact that the relation between ingoing and outgoing waves is a simple phase shift is a consequence of the invariance of $u(r,\theta)$ in $\varphi$ and of the approximation that $|\mathbf{L}|$ is conserved and that there is no absorption. Otherwise, a general $S$ matrix would be necessary. We thus want to describe the semiclassical limit of the effect of such a potential on a wave function corresponding to an angular momentum pointing toward direction $(\theta_i,\phi_i)$.

Such a state is, according to Edmonds[32]:

$$\begin{aligned}|L,\theta_i,\varphi_i\rangle&=R(\varphi_i,\theta_i,0)|L,L\rangle\\&=\sum_m Y_L^m(\theta,\varphi)R^L_{mL}(\varphi_i,\theta_i,0)\\&=\sum_m Y_L^m(\theta,\phi)e^{-im\varphi_i}r^L_{mL}(\theta_i)\end{aligned} \tag{A3}$$

(where $R$ and $r$ are the rotation matrices defined by Messiah[31]).

This is because the state $|L,L\rangle$ is a minimum extension wave packet constrained by the uncertainty relation

$$\Delta L_x\Delta L_y\geqslant 1/2\langle L_z\rangle \tag{A4}$$

since for a state $|LM\rangle$:

$$\Delta L_x\Delta L_y=1/2[L(L+1)-m^2] \tag{A5}$$

attains its minimum value (A4) only for $m=L$. This wave packet's extension goes to zero in relative value as $L\to\infty$, and this property is kept by the state $|L\theta_i\varphi_i\rangle$ defined by Eq. (A3), but not by an ordinary $|Lm\rangle$ state.

The ingoing wave will thus be

$$\psi^{(-)}(r,\theta,\varphi;L\theta_i\varphi_i)=u_L^{(-)}(r)a_L\sum_m\frac{Y_L^m(\theta,\varphi)}{kr}e^{-im\varphi_i}r^L_{mL}(\theta_i), \tag{A6}$$

where the $a_{Lm}$ are chosen equal to $a_Le^{-im\varphi_i}r^L_{mL}(\theta_i)$, where $a_L$ is independent of $m$. The effect of diffusion is, according to Eq. (A2), to multiply the ingoing wave by a phase factor $e^{2i\sigma_L}\times e^{2i\delta_{Lm}}$, giving an outgoing wave

$$\psi^{(+)}(r,\theta,\varphi;L\theta_i,\varphi_i)=u_L^{(+)}(r)e^{2i\sigma_L}a_L\sum_m\frac{Y_L^m(\theta,\varphi)}{kr}e^{-i(m\varphi_i-2\delta_{Lm})}r^L_{mL}(\theta_i). \tag{A7}$$

For large $L$, $r^L_{mL}(\theta_i)$ will be nonzero only for a narrow range of $m/L$ around $m_i/L=\cos\theta_i$, whose width goes to zero as $L\to\infty$, as can be checked directly on its explicit formula.[32] $\delta_{Lm}$ can thus be developed in the neighborhood of $m=m_i$ as

$$\delta_{Lm} = \delta_{Lm_i} + (m - m_i)\left(\frac{d\delta_{Lm}}{dm}\right)_{m=m_i}$$
$$= c_{Lm_i} + m\delta'_{Lm_i}$$

with

$$\delta'_{Lm_i} = \left(\frac{d\delta_{Lm}}{dm}\right)_{m=m_i} \text{ and } c_{Lm_i} = \delta_{Lm_i} - m_i\delta'_{Lm_i}. \quad \text{(A8)}$$

Thus

$$e^{-i(m\varphi_i - 2\delta_{Lm})} = e^{2iC_{Lm_i}} e^{-im(\varphi_i - 2\delta'_{Lm_i})}. \quad \text{(A9)}$$

The outgoing wave has thus a $\theta,\varphi$ dependance corresponding to an angular momentum pointing in output direction:

$$\theta_0 = \theta_i, \varphi_0 = \varphi_i - 2\left(\frac{d\delta_{Lm}}{dm}\right)_{m=m_i}. \quad \text{(A10)}$$

There is, in addition, a phase factor $e^{2iC_{Lm_i}}$ which is unimportant in the present case, but which would be essential of course in dealing with an ingoing wave which would be a superposition of several $L$ or several $\theta_i,\varphi_i$. Notice in this context, that the present results are independent of the direction of the main axis of the classical ellipse in the plane perpendicular to **L**. The reason is that, since no component of the Runge Lenz vector $\mathbf{L}_\wedge \mathbf{p} - \mathbf{p}_\wedge \mathbf{L} - \mathbf{r}/r$ (which is the constant of motion which defines the ellipse's axis) commutes with $\mathbf{L}^2$, selecting a given value of $L$ is inconsistent with any fixed direction for this axis. Selecting a wave packet which gives a fixed direction of the ellipse axis would need to use an ingoing wave function which would be a proper combination of several $L$ waves. This would complicate the calculations, but it is not necessary in the present context, since we want to compare results between a quantum system and its true semiclassical limit. The fact that this quantum system is not what we imagine for a classical orbit is unimportant because the classical mechanics must fail somewhere in describing a molecule, since a molecule would not be stable in the classical limit. With the notations of the text, $m = \Lambda$ and $\delta_{Lm} = \pi\mu_{L\Lambda}$.

The conclusion of this Appendix is thus that the interaction between the Rydberg electron and the ion core is described by a rotation of **L** around the $Na_2^+$ ion axis by an angle

$$\delta\varphi = \varphi_0 - \varphi_i = -2\pi\frac{\partial\mu}{\partial\Lambda}. \quad \text{(A11)}$$

So that, with

$$\mu = \mu_0 - \frac{K}{4\pi L}\Lambda^2, \quad \delta\varphi = K\frac{\Lambda}{L} = K\cos\theta. \quad \text{(A12)}$$

## APPENDIX B: THE $(\theta,\varphi)$ POINCARÉ MAP

Let $(\theta,\varphi)$ be the polar angles of $L$ with respect to the molecular $z$ axis $(\alpha,\beta)$ its polar angle with respect to $x(N^+)$ axis (Fig. 1). They are related through their projection on three axes:

$$Ox \Rightarrow \cos\alpha = \sin\theta\cos\varphi,$$
$$Oy \Rightarrow \sin\alpha\cos\beta = \sin\theta\sin\varphi, \quad \text{(B1)}$$
$$Oz \Rightarrow \sin\alpha\sin\beta = \cos\theta.$$

We will use subscripts 0 for initial state (immediately after a collision), 1 for intermediate state after a revolution of the electron in its orbit, 2 for final state after the next collision. Let $E_e$ be the energy [in atomic units (a.u.) = 2 Rydbergs] of the electron in its orbit. Its period is $T_e = 2\pi(-2E_e)^{-3/2}$. Let $E_N = N^2/2I$ be the energy of the rotator (molecular ion core) of angular momentum $N$ (we drop the superscript of $N^+$ in this Appendix) and moment of inertia $I$. Its period is $T_N = 2\pi I/N$. There is a resonance when $T_e/T_N$ is an integer multiple of 1/2, so that there is an integer number of half-turns of the core during the electron orbit.

Let $E = E_e + E_N$ the total energy (conserved), and $J = N + L$ the total angular momentum (conserved also). $L = |\mathbf{L}|$ is supposed conserved, but not $N = |\mathbf{N}|$ which is related to polar angles through

$$J^2 = N^2 + L^2 + 2LN\cos\alpha \quad \text{(B2)}$$

and thus vary between the limits $J - L$ and $J + L$ after each collision. Its initial value $N_0$ (defined by given $\theta_0$ and $\varphi_0$) is computed from Eqs. (B2) and (B1). $T_N = 2\pi I/N_0$, $E_e = E - E_N$, and $T_e = 2\pi(-2E_e)^{-3/2}$ are then deduced. During the electron orbit, **L** is fixed in laboratory frame and the ion core precesses counterclockwise around **N**. In the molecular frame thus, **L** precesses clockwise around the $x$ axis. Thus,

$$\alpha_1 = \alpha_0, \quad \beta_1 = \beta_0 - 2\pi T_e/T_N. \quad \text{(B3)}$$

Values for $\theta_1$ and $\varphi_1$ are deduced from Eqs. (B3) and (B1).

During the collision, **L** precesses around the $Oz$ axis by an angle

$$\delta\varphi = K\cos\theta_1. \quad \text{(B4)}$$

This angle must be odd in the symmetry $\theta_1 \to \pi - \theta_1$. This is due to the symmetry of the Hamiltonian in a reflexion through any plane containing $Oz$ (Kronig's symmetry). Indeed, taking into account that **L** is an axial vector, a reflection in the $xOz$ plane makes $\theta \to \pi - \theta$ and $\varphi \to \pi - \varphi$, and thus $\delta\varphi \to -\delta\varphi$.

Due to the conservation of $\mathbf{J} = \mathbf{N}_1 + \mathbf{L}_1 = \mathbf{N}_2 + \mathbf{L}_2$, the molecular reference frame is not fixed during the collision, but it precesses by an angle $\delta\varphi' = (ON_2, ON_1)$ around the $Oz$ axis. The $Oz$ axis itself is fixed because the component of **L** along this axis is fixed. Thus $\theta_2 = \theta_1$. The final value of $\varphi_2$ is obtained in writing the conservation law $\mathbf{N}_1 + \mathbf{L}_1 = \mathbf{N}_2 + \mathbf{L}_2$ in the *initial* molecular reference frame

$$L\sin\theta_1\cos\varphi_1 + N_1 = L\sin\theta_2\cos(\varphi_1 + \delta\varphi) + N_2\cos\delta\varphi',$$
$$L\sin\theta_1\sin\varphi_1 = L\sin\theta_2\sin(\varphi_1 + \delta\varphi) + N_2\sin\delta\varphi', \quad \text{(B5)}$$
$$L\cos\theta_1 = L\cos\theta_2.$$

The set of two first equation is solved for two unknowns $N_2$ and $\delta\varphi'$, and one deduces $\varphi_2 = \varphi_1 + \delta\varphi' + \delta\varphi$ in the *final* reference frame. In doing so, care must be taken not to compute separately sine and cosine of the same angle, this would lead to bad divergence due to roundoff errors.

[1] *Quantum Chaos and Statistical Nuclear Physics*, edited by T. H. Seligmann and H. Nishioka, Lecture Notes in Physics No. 263 (Springer, Berlin, 1986).

[2]*Chaotic Behavior In Quantum Systems*, edited by G. Casati (Plenum, New York, 1985).
[3]M. V. Berry, in *Chaotic Behavior of Deterministic Systems. Les Houches, Session XXXVI, 1981*, edited by G. Iooss, R. H. G. Helleman, and R. Stora (North-Holland, Amsterdam, 1983).
[4]E. J. Heller and R. L. Sundberg in Ref. 2; E. J. Heller, Faraday Discuss. Chem. Soc. **75**, 141 (1983), and references therein; E. B. Stechel and E. J. Heller, Annu. Rev. Phys. Chem. **35**, 563 (1984).
[5]Y. Alhassid and R. D. Levine, Phys. Rev. Lett. **57**, 2879 (1986); R. D. Levine, Adv. Chem. Phys. **70**, 53 (1987).
[6]K. K. Lehmann and S. L. Coy, J. Chem. Phys. **83**, 3290 (1985); S. L. Coy, K. K. Lehmann, and F. C. De Lucia, *ibid.* **85**, 4297 (1986).
[7]O. Bohigas, M. J. Giannoni, and C. Schmit, Phys. Rev. Lett. **52**, 1 (1984).
[8]P. Pechukas, Phys. Rev. Lett. **51**, 943 (1983).
[9]M. V. Berry, Proc. R. Soc. London Ser. A **400**, 229 (1985).
[10]P. Labastie, M. C. Bordas, B. Tribollet, and M. Broyer, Phys. Rev. Lett. **52**, 1681 (1984); M. C. Bordas, M. Broyer, J. Chevaleyre, P. Labastie, and S. Martin, J. Phys. **46**, 27 (1987).
[11]U. Fano, Phys. Rev. A **2**, 353 (1970); J. Opt. Soc. Am. **65**, 979 (1975).
[12]C. H. Greene and Ch. Jungen, Adv. At. Mol. Phys. **21**, 51 (1985).
[13]Ch. Jungen and O. Atabek, J. Chem. Phys. **66**, 5584 (1977).
[14]E. P. Wigner, Oak Ridge National Laboratory, Report No. ORNL-2303, 1956 (unpublished); reprinted by C. E. Porter, in *Statistical Theories of Spectra: Fluctuations* (Academic, New York, 1965), p. 139.
[15]T. A. Brody, J. Flores, J. B. French, P. A. Mello, A. Pandey, and S. S. Wong, Rev. Mod. Phys. **53**, 385 (1981).
[16]M. L. Mehta, *Random Matrices and the Statistical Theory of Energy Levels* (Academic, New York, 1967).
[17]L. Leviandier, M. Lombardi, R. Jost, and J. P. Pique, Phys. Rev. Lett. **56**, 2449 (1986).
[18]J. P. Pique, Y. Chen, R. W. Field, and J. L. Kinsey, Phys. Rev. Lett. **58**, 475 (1987).
[19]M. Bixon and J. Jortner, J. Chem. Phys. **50**, 3284 (1969).
[20]F. Lahmani, A. Tramer, and C. Tric, J. Chem. Phys. **60**, 4431 (1974); J. M. Delory and C. Tric, Chem. Phys. **3**, 54 (1974).
[21]M. V. Berry and M. Tabor, Proc. R. Soc. London Ser. A **356**, 375 (1977).
[22]M. C. Gutzwiller, J. Math. Phys. **8**, 1979 (1967); **10**, 1004 (1969); **11**, 1791 (1970); **12**, 343 (1971); Phys. Rev. Lett. **45**, 150 (1980); Physica D **7**, 341 (1983).
[23]R. Balian and C. Bloch, Ann. Phys. **69**, 76 (1972); **85**, 514 (1974).
[24]S. W. Mc Donald and A. N. Kaufman, Phys. Rev. Lett. **42**, 1189 (1979); M. V. Berry, Ann. Phys. **131**, 163 (1981); M. Robnik, J. Phys. A **17**, 1049 (1984).
[25]G. Casati, B. V. Chirikov, and I. Guarneri, Phys. Rev. Lett. **54**, 1350 (1985).
[26]M. Robnik, J. Phys. A **17**, 1049 (1984).
[27]J. N. Mather, Ergodic Theory Dynam. Sys. **2**, 3 (1982).
[28]K. K. Lehmann, G. J. Scherer, and W. Klemperer, J. Chem. Phys. **76**, 6641 (1982); **78**, 608 (1983); D. Farrely and W. P. Reinhardt, *ibid.* **78**, 608 (1983).
[29]G. Casati and I. Guarneri, in Ref. 1, p. 238.
[30]W. P. Reinhardt, *Mathematical Analysis of Physical Systems*, edited by R. E. Mickens (Van Nostrand Reinhold, New York, 1985), p.169.
[31]A. Messiah, *Mécanique Quantique* (Dunod, Paris, 1962).
[32]A. R. Edmonds, *Angular Momentum in Quantum Mechanics* (Princeton University, Princeton, NJ, 1974).